TRANSNAV
http://www.transnav.eu
the International Journal
on Marine Navigation
and Safety of Sea Transportation
Volume XX
Number X
XXXXXXXXX 202X

DOI: 10.12716/1001.XX.XX.XX

Tools for Optimizing Performance of VOYages at Sea

J.A. Johannessen[1], A. Perrin[1], L. Gaultier[2], S. Herlédan[2], C. Pouplin[2], F. Collard[2], J.P.Maze[3], M. Dussauze[3], J. Rapp[4], R. Fanebust[5], S. Andersen[5], O. Franks[6] & R. Meyer[7]
[1] *Nansen Environmental and Remote Sensing Center, Bergen, Norway*
[2] *OceanDataLab, Plouzané, France*
[3] *Actimar, Brest, France*
[4] *CMA-CGM, Marseille, France*
[5] *Grieg Star, Bergen, Norway*
[6] *Nelson Mandela University, Port Elisabeth, South Africa*
[7] *CSIR, Cape Town, South Africa*

ABSTRACT: The aim of the TOPVOYS project supported by the MarTERA ERA-Net Cofund program within the European Commission is to advance and implement analyses tools and decision support system for voyage optimisation. Based on marine weather analyses and forecasts combined with near real time satellite-based observations of wind, wave and surface current conditions as well as sea surface temperature fields the best shipping route are examined. The proposed approach aims to identify the optimum balance between minimisation of transit time and fuel consumption as well as reduction of emissions without placing the vessel at risk to damage and or crew injury. As such it is compliant with the International Maritime Organization guidelines [6] for ship routeing to keep the traffic smooth and avoid accidents, notably in the presence of unfavorable marine meteorological conditions. The tool performances will be demonstrated both in post-voyage analyses and real time operations for the North Atlantic Ocean crossings, voyages from Europe through the Mediterranean Sea and the Suez Channel to the Far East (e.g. China, South Korea) and voyages around Southern Africa.

1 INTRODUCTION

The recent decade has seen a increasing development in ship routeing services whereby more reliable weather conditions, sea states and surface currents are taken into account (e.g. [3, 13, 11]). Optimum ship routing means the "best route" for a ship based on the marine weather forecasts including wave and surface current conditions, ship characteristics and cargo requirements. For most voyages this will mean the minimum transit time that avoids significant risk to the vessel, crew and cargo. The goal is not to avoid all adverse weather, waves and current conditions but to find the best balance to minimize time of transit and fuel consumption without placing the vessel at risk to damage or crew injury. In recent years concern regarding CO2 emission from ships has also emerged and should therefore preferably be taken into account regarding ship routing and voyage optimization (e.g. [7, 8]).

In this paper we will present preliminary results of the investigation and development of tools for optimizing performance of voyages at sea (TOPVOYS project) funded by the MarTERA EraNet Co-fund program for a 3-year period from 2018-2021. The data is outlined in section 2, followed by the approach for the development of the routing optimization tool in Section 3. Section 4 describes the validation method and the summary is provided in Section 5.

2 DATA AND APPROACH

The types of data and information products considered necessary for provision of reliable and optimized ship routing can be grouped into marine weather data, model forecast fields, near real time satellite data and in-situ measurements. Regarding the satellite data there is a wide range of oceanic variables that will be used to retrieve and validate the surface currents and frontal structures as indicated in Table 1, including sea surface temperature (SST), chlorophyll (Chl) observations, surface geostrophic current, significant wave height and wave length and propagation direction.

Table 1. Key satellite sensor data (level, resolution, provider). Note that radar altimeter data (wave height) are available in the CMEMS multi-observation data set.

Sensor	Product	Level	Resolution	Data Provider
Sentinel-3 SLSTR SST and SEVIRI	Sea surface temperature/fronts	L2	~ 1 km	EUMETSAT
Sentinel-3 OLCI Chl	Chlorophyll/fronts	L2	~ 300 m	EUMETSAT
Sentinel-3 and Jason altimeters	Surface geostrophic current/fronts	L3	~ 10 km	CLS/Salto Duacs
Sentinel-3 and Jason altimeters	Significant wave height	L3	~ 10 km	CLS/Salto Duacs
Sentinel-2 spectral imager	Wave length - direction/glitter	L2	~ 1 km	ODL
Sentinel-1 A/B SAR	Wave length - direction	L2	~ 1 km	Scihub/ESA
Sentinel-1 SAR Doppler shift	Radial surface current	L3	~ 2 km	Scihub/ESA
CMEMS-Multi-Obs (Global)	All above from Sentinel-3	L3/L4	~ 10 km	CMEMS

Table 2. In-situ sensor data and providers

Sensor	Key products/resolution	Coverage	Data providers
HF radars	Surface current/ order km	surface	EMODNET PHYSICS
Loch (ship-based)	Surface current/ tens of meters	surface	CMA CGM (Watch Report)
Argo	Surface current/ ~100 m	surface	CMEMS, Coriolis
Surface drifting buoys	Current/~100m	15m depth	CMEMS, Coriolis

Table 3. Complementary model-based surface current fields. *The GlobCurrent fields is an interpolated regular global surface current product derived from satellite data. Geostrophic balance and Ekman current estimation applied.

Product	Coverage	Resolution	Model	Provider
CMEMS-GLOBAL	global	~ 8 km	NEMO	CMEMS
RTOFS	global	~ 8 km	HYCOM	NOAA
GOFS	global	~ 8 km	HYCOM	NRL
MED-CMEMS	Mediterranean Sea	~4 km	NEMO	CMEMS
IBI	Iberian Peninsula & Bay of Biscay	~2 km	NEMO	CMEMS
GlobCurrent*	global	~ 25 km	Geo/Ekman	CMEMS
Wave Model	global	~ 10 km	MFWAM	MeteoFrance

Importantly, these satellite data can often be complemented and collocated with in-situ data allowing comparison of the surface current and frontal structures derived from the satellite data to the Argo floats, surface drifter data, HF-radars and on-board estimates of surface currents as shown in Table 2.

Finally, the satellite and in-situ based observation data are combined and extended with surface current and wave field forecast products offering global and regional coverages at spatial resolutions ranging from 25 km to 2km as shown in Table 3.

A major innovation in this project is the systematic use of satellite observations of the marine environment in near real time to generate information products tailored to ship locations and their planned course for the next 24 hours. Presently, the joint EU-ESA Copernicus program (https://marine.copernicus.eu) ensures routine access to the sea surface current, significant wave height, wave spectra and sea surface temperature derived from the Sentinel satellite missions (see Table 1). These variables, in turn, allows the identification and location of meandering surface current frontal boundaries and eddies, evidence of wave-current interactions and presence of crossing seas.

Satellite data regularly collected over time is also highly useful to establish climatology that function as reference conditions for assessing the magnitude of the departure of the near real time product from the climatology mean. This is illustrated in Figure 1 displaying the 4-year mean of significant wave height, significant wave height gradient and surface geostrophic current vorticity (estimated from the gradient in meridional minus zonal current). Not surprisingly the roughest sea state conditions are found in the Southern Ocean with a mean significant wave height between 4 and 5 m. In comparison, the mean significant wave height in the North Atlantic and North Pacific respectively ranges between 3-4 m and 2-3m.

On the other hand, when looking at the mean of the significant wave height gradient and the surface geostrophic current vorticity the pictures largely change towards the manifestation of the boundaries of the basin-scale surface current system such as the Gulf Stream, the Kuroshio Current and the greater Agulhas Current, known to reach surface current speeds of 1-2 m/s. These intense current regimes are recognized with strong mesoscale and sub-mesoscale variabilities that have large influence on the sea state, in particular due to the change in wave heights invoked by wave refraction from the spatially varying surface current [9]. As noticed in Figure 1, the two fields show a significant degree of collocated expressions of distinct anomalies in both the significant wave height gradient and surface geostrophic current vorticity. This is a key indicator of strong wave-current interaction, notably caused by:

- refraction of the longer waves (> 200 m) as they propagate across the surface current boundaries and feel the significant change in surface geostrophic current and associated vorticity field;
- steepening of the waves and in particular the shorter wind waves (< 50 m) as they propagate against the strong surface currents.

Wave refractions by the surface current are observed in both Sentinel-1 Synthetic Aperture Radar (SAR) images and Sentinel-2 multispectral images (under cloud free conditions) revealing both the incident wavelength and direction and their changes when propagating across the surface current

boundaries. Moreover, complementary collocated observations from Sentinel-3 deliver measurements of the surface current and sea surface temperature (under cloud free conditions).

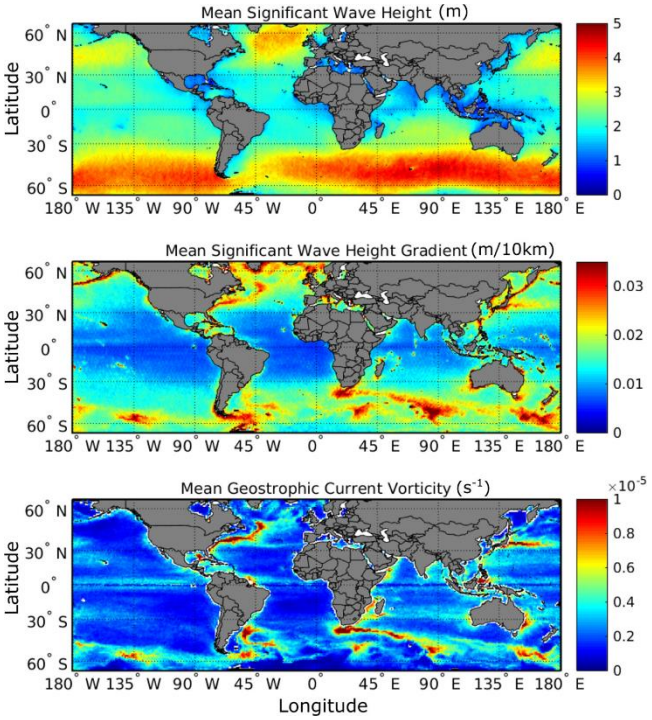

Figure 1. 4-year mean (2013–2016) for significant wave height (top), significant wave height gradient (middle) and surface geostrophic current vorticity (lower) computed using the constellation of 4 satellite altimeters and projected on a 0.5° * 0.5° grid. The color bars mark the value in the given units.

An example of multi-sensor satellite-based observations of the spatial variability in the significant wave height, the wave propagation direction and the surface geostrophic current blended with swell propagation simulations is shown in Figure 2 with focus on the core of the Agulhas Current.

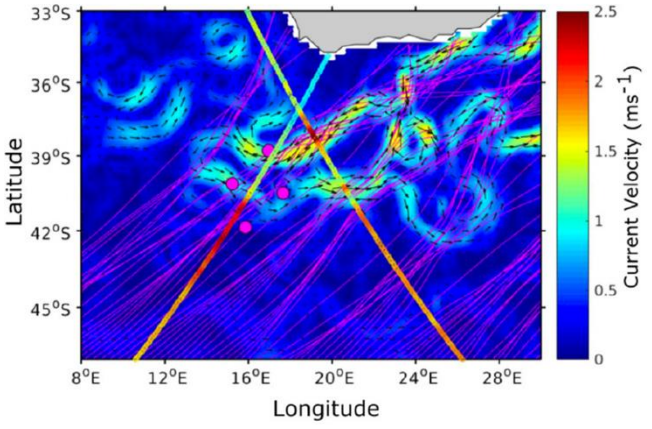

Figure 2. Daily surface geostrophic currents on 2016.02.28 (velocity as black arrows). The magenta lines map the swell propagation rays. The magenta circles give the Sentinel-1 wave-mode images location the same day. Two Jason-2 altimeter tracks are shown, whose significant wave height values are normalized to fit the current scale [12].

Evidence of altimeter-based observations of strong wave-current interactions are clearly depicted in which increased significant wave height are collocated with areas of intense surface geostrophic currents, in particular for the opposing currents such as seen near the retroflection region of the Agulhas Current centered around 39°S and 18°E. The complementary simulated wave-current refraction are highly in consistence with these observations and reveals how the refractions lead to changes in wave propagation and the set-up of crossing seas. The importance of the wave-current interaction can also be explored from the model simulations as highlighted by the comparison of the significant wave height field with and without the presence of the surface current (see Figure 3). As noticed the significant wave height is enhanced by around 50% in the core of the Agulhas Current. Hence, the convergence (growth) of wave energy (higher sea states) and directional spreading (dangerous crossing seas) can be located both from the observations and the model simulations leading to a more reliable assessment of potential navigational risk areas. The assessment may also yield more confidence in model predicted sea state and location of unwanted extreme waves.

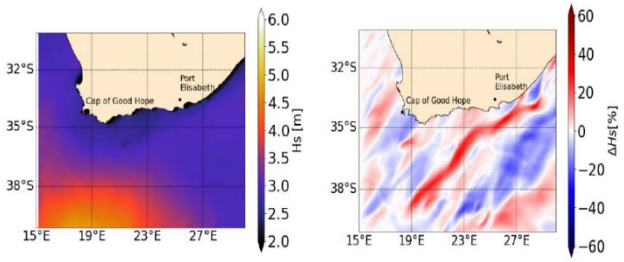

Figure 3. Significant wave height from WW3 sea state model for Sept 9, 2015 at 0h UTC. (left) without surface current; (right) relative variations of significant wave height (⊚Hs) when considering surface current from the CMEMS operational Mercator model (from [9] pers. com).

3 DEVELOPMENT OF THE ROUTING OPTIMIZATION TOOL

An innovative tool aiming at providing value-added surface current products currently tailored to the Mediterranean Sea, North Indian Ocean, East Asia seas, North Atlantic, South Atlantic and seas around Southern Africa is under development and testing. The products are provided both from available forecasts and from observations. A series of post-processing routines have been developed in order to help the ocean forecaster build the optimized surface current forecast. Different proxies have been defined to qualify the surface current forecast performances at each in-situ measurement location. Moreover, the comparison of models with satellite derived sea surface temperature and surface geostrophic current is used to assess the ability of the ocean models to locate the mesoscale structures (e.g. eddies, meanders fronts). This analysis provides comparison scores ranging from 1 (poor) to 5 (excellent) and is tailored to both current direction and current magnitude as indicated below.

These scores are established automatically through comparison with direct current estimation made on the bridge (e.g. Watch Reports), with surface drifters

and visually by comparison with SST field. The closer the score is to 5, the better is the agreement between the forecast product and the observations. Hence, according to the scores within a subregion, the routing software (ACTIROUTE) proposes an optimized and qualified surface current field used by external software to select the most preferred route. Otherwise, the most direct route is followed. In order to facilitate the decision support for the operator which makes the analysis of the performance of the various forecast products, the current maps from the different products can be overlaid and displayed in the same SEAScope visualization portal. The operator can then quickly verify if the products and observations are coherent. In the same way, the scores obtained by comparing the forecast products to the observations are saved in a format readable by SEAScope.

4 VALIDATION

In the TOPVOYS study, new diagnostics have been implemented to validate surface currents using tracer observations such as the sea surface temperature and the Chlorophyll. The position of the dynamical current structures can then be assessed when a satellite-based SST or Chlorophyll map is available. The frontal structures are extracted from the tracer image and compared with the Lagrangian Coherent Structures derived from the surface currents. To extract the frontal structures, an algorithm consistent with [1] and [2] is implemented to locate the position of the fronts as schematically illustrated in Figure 4. For each moving window, a histogram is used to detect different population. The points that are separating the two population are considered as the representation of the surface front. For each point, a probability of having a front is then estimated by counting the number of times it has been detected on the moving window. A contour-following processing on the probability for the presence of the front is then performed to reconstruct the frontal structures.

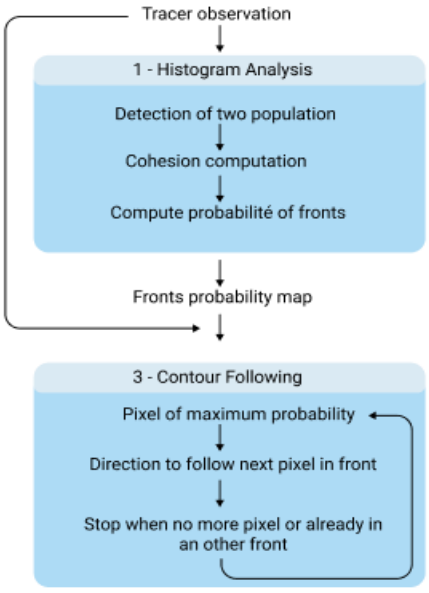

Figure 4. Algorithm for extraction of fronts from a tracer image

Next, in order to compare the frontal structure with the different available velocity products it is necessary to compute a proxy for each velocity product using the Finite-Size Lyapunov Exponent (FSLE) to reveal the possible position of the tracer gradient in the velocity field (e.g. [5, 10]). From the FSLE image a contour following algorithm is then applied to retrieve the corresponding frontal structures followed by a comparison to the corresponding fronts derived in the tracer image as shown in Figure 5. This yield estimates of the distance between the fronts as well as the differences in curvature and direction and enables the selection of the best velocity for each points along the front.

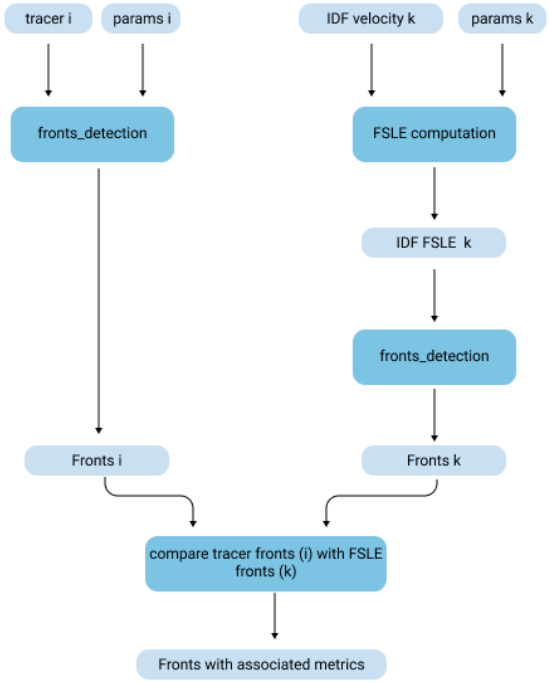

Figure 5. Validation of the velocity field (k) using the tracer image (i)

An example of the practical use of this validation tool is shown in Figure 6. This is based on reconstruction of a surface current field from the satellite-based SST frontal maps (derived from SEVIRI) followed by an interpolation onto the grid of the surface current products derived from GlobCurrent. The two surface current maps are then compared and assessed for consistency and accuracy. Only points containing frontal information are used for this validation. The comparison demonstrates that the mesoscale anticyclonic eddy is satisfactorily positioned in both fields although there are slight differences in both surface current magnitudes and directions.

In the following a more comprehensive test case is presented for the region extending from the Gulf of Aden to the East of the Socotra Island. This area (see Figure 7) encompasses various hydrodynamic features (frontal areas, mesoscale eddies, meandering currents) that in some cases may require a potential change in routing. The challenge is thus to precisely locate the position of these features. Hence, the comparison shall preferably enable the assessment of the different products in terms of quality and reliability in order to select the best route.

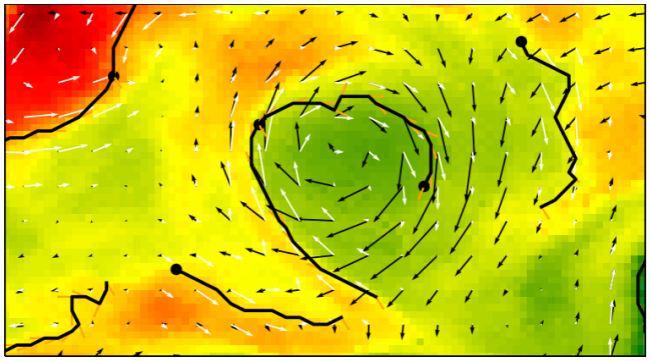

Figure 6. Comparison of independent surface current fields. The white arrows represent the surface current field derived from the SST frontal map and re-interpolated on the grid to validate against the black arrows independently derived from the GlobCurrent products.

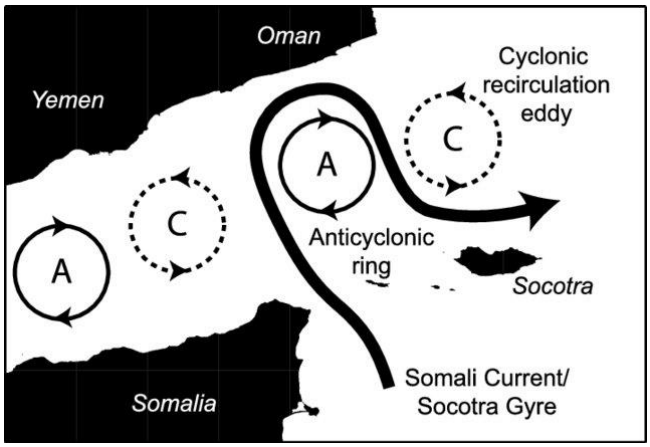

Figure 7. Schematic hydrodynamic features in the mouth of the Gulf of Aden (extracted from [4] revealing presence of anticyclonic (A) and cyclonic (C) eddies and meandering surface currents.

The results of the comparison between the FSLE retrieved from different observation-based and model-based surface current velocity fields and the SST fronts derived from the SEVIRI product in the North-West of the Arabian Sea in February 2021 are shown in Figure 8. Inside the Gulf of Aden (yellow square), the fronts detected from the SEVIRI SST display the edges of two rings (consistent with structures in Figure 7). The distances between these SST-based fronts and the FSLE-based fronts are smaller for the HYCOM product (~20 km: blue/green color) than for Mercator or the Total Current derived from observations (~80-100 km: brown color). This implies that HYCOM model should be considered for the routing in this area. In contrast, at the mouth of the Gulf of Aden (red rectangle), the distance between the FSLE computed from the Mercator model field and the fronts detected from SEVIRI is on average smaller than the other two products.

The routing (following the ACTIROUTE software) will update its optimization procedure with these new observations (SST) by considering the metrics retrieved from the comparison between FSLE-based and SST-based frontal locations, orientation, structures and curvatures. In particular, it will penalize the local products with larger separation distance between the observed-based and model-based fronts. This work is still under progress.

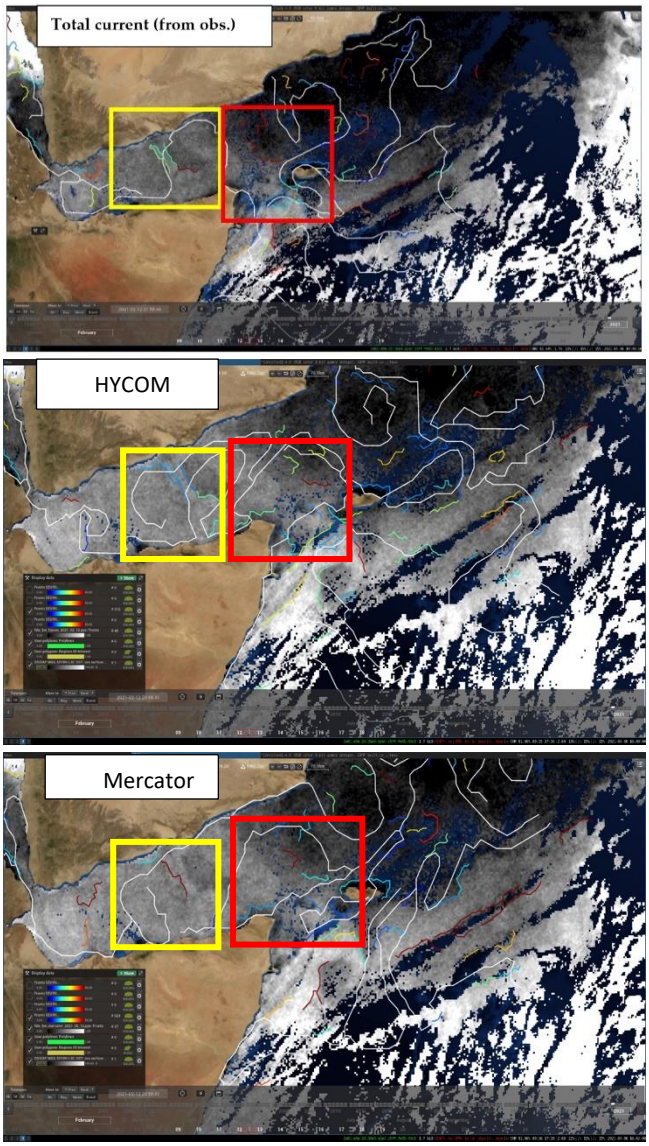

Figure 8. Comparison between the FSLE-based fronts (white lines) and the observed SST-based fronts (colour). The colour represents the distance from SST to FSLE based fronts from dark blue (0 km) to dark red (80 km). Each line represents the result of one velocity field: FSLE based fronts from the observed total surface current (top), from the HYCOM model (middle) and from the MERCATOR model (bottom) The background grey-scale image is from the SEVIRI L3 SST product (missing data due to cloud cover).

5 SUMMARY

In this paper we have used near real time satellite data and in-situ data of the surface current and sea surface temperature fields for assessment and optimization of the surface current field for ship routing. It has been demonstrated that synoptic maps of surface frontal structures provide highly important products and information on meandering patterns and motions which are proxy for the surface currents dynamics, and as such allowing assessment and validation on the quality of the delivered surface current products with emphasis on the upper 10 to 20 m. Moreover, regular use of wave ray-tracing model with different surface currents will be run for simulations of rapidly changing and possibly occurrences of extreme waves invoked by wave-current interaction.

The ultimate goal is to advance the development of a decision support system for optimization of ship routing that provides a reliable traffic-light system by which indices for the pre-selected ship routes builds on regular near real time updates of:

- meandering fronts and eddies;
- rapidly changing currents;
- evolving wind sea and swell fields;
- likelihood of wave energy focusing caused by wave-current interaction;
- likelihood of crossing seas;
- likelihood of dangerous waves.

The provision of these indices will be based on the combination satellite-based and and-situ based data sources and model fields including:

- surface current from the GlobCurrent database;
- model-based surface current (CMEMS, etc)
- sea state from wave models with and without wave-current interaction;
- altimeter derived significant wave height data;
- Sentinel-1 SAR-based wave mode and interferometric wide acquisitions;
- Satellite-based sea surface temperature fields;
- ECMWF wind field and wind stress

REFERENCES

1. Cayula, J.-F., Cornillon, P.: Edge Detection Algorithm for SST Images. Journal of Atmospheric and Oceanic Technology. 9, 1, 67–80 (1992). https://doi.org/10.1175/1520-0426(1992)009<0067:EDAFSI>2.0.CO;2.
2. Cayula, J.-F., Cornillon, P.: Multi-Image Edge Detection for SST Images. Journal of Atmospheric and Oceanic Technology. 12, 4, 821–829 (1995). https://doi.org/10.1175/1520-0426(1995)012<0821:MIEDFS>2.0.CO;2.
3. Chang, Yu-Chia , Ruo-Shan Tseng, Guan-Yu Chen, Peter C Chu and Yung-Ting Shen (2013), Ship Routing Utilizing Strong Ocean Currents, *The Journal of Navigation* (2013), 66, 825–835. © The Royal Institute of Navigation 2013, doi:10.1017/S0373463313000441.
4. Fratantoni, D.M., Bower, A.S., Johns, W.E., Peters, H.: Somali Current rings in the eastern Gulf of Aden. Journal of Geophysical Research: Oceans. 111, C9, (2006). https://doi.org/10.1029/2005JC003338.
5. Gaultier, L., Verron, J., Brankart, J.-M., Titaud, O., Brasseur, P.: On the inversion of submesoscale tracer fields to estimate the surface ocean circulation. Journal of Marine Systems. 126, 33–42 (2013). https://doi.org/10.1016/j.jmarsys.2012.02.014.
6. International Maritime Organization (IMO) IG927E Ships' Routeing, 14th Edition 2019, IM927, ISBN: 978-92-801-0049-5 (9789280100495).
7. International Maritime Organization (2010). Reduction of GHG emissions from ships, IMO-MEPC 61/INF.22, 2 August 2010.
8. Kim, J.-G., Kim, H.-J., and Lee, P. T. W (2013). "Optimising container ship speed and fleet size under a carbon tax and an emission trading scheme." *International Journal of Shipping and Transport Logistics*, vol. 5, no. 6, pp. 571–590. DOI: 10.1504/IJSTL.2013.056835.
9. Marechal, G., Ardhuin, F.: Surface currents and significant wave height variability: a numerical investigation of the Agulhas current region. Earth and Space Science Open Archive. 18 (2020). https://doi.org/10.1002/essoar.10503641.1.
10. d'Ovidio, F., Fernández, V., Hernández-García, E., López, C.: Mixing structures in the Mediterranean Sea from finite-size Lyapunov exponents. Geophysical Research Letters. 31, 17, (2004). https://doi.org/10.1029/2004GL020328.
11. Pennino, Silvia, Salvatore Gaglione, Anna Innac, Vincenzo Piscopo and Antonio Scamardella (2020), Development of a New Ship Adaptive Weather Routing Model Based on Seakeeping Analysis and Optimization, *J. Mar. Sci. Eng.* 2020, 8, 270; doi:10.3390/jmse8040270.
12. Quilfen, Y., Chapron, B.: Ocean Surface Wave-Current Signatures From Satellite Altimeter Measurements. Geophysical Research Letters. 46, 1, 253–261 (2019). https://doi.org/10.1029/2018GL081029.
13. Yang, Liqian , Gang Chen, Jinlou Zhao and Niels Gorm Malý Rytter (2020), Ship Speed Optimization Considering Ocean Currents to Enhance Environmental Sustainability in Maritime Shipping, *J. Mar. Sci. Eng.* 2020, 8, 270; doi:10.3390/jmse8040270.